J. Min. Metall. Sect. B-Metall., 56 (1) (2020) 77 - 87

Journal of Mining and Metallurgy, Section B: Metallurgy

A NEW APPROACH TO SYNTHESIZE NANO-YTTRIUM BORIDE PARTICLE THROUGH METALLOTHERMIC REDUCTION PROCESS

M. Sadhasivam [a], L. J. Berchmans [b], G. K. Meenashisundaram [c], U. Mehana Usmaniya [b], S. R. Sankaranarayanan [a,*], S.P. Kumaresh Babu [a]

[a] National Institute of Technology, Department of Metallurgical and Materials Engineering, Tiruchirappalli, Tamilnadu, India

[b] Council of Scientific and Industrial Research-Central Electro Chemical Research Institute, Electropyro Metallurgy Division, Karaikudi, Tamilnadu, India

[c] Singapore Institute of Manufacturing and Technology, Forming technology group, Singapore

(Received 15 March 2019; accepted 16 September 2019)

Abstract

In the present study, a novel attempt is made to synthesize yttrium boride (YB_4) nano-sized powders through metallothermic reduction method. The starting materials used were yttria (Y_2O_3) and boron oxide (B_2O_3) as reactants, and calcium (Ca) as reductant. The reaction was carried out at 950^0C under argon atmosphere followed by acid washing. The product was subjected to X-ray fluorescence (XRF) which indicated its elemental constituents and purity of the prepared nanopowders. X-ray diffraction (XRD) studies revealed the formation of YB_4 and YB_6 phases as well as their respective crystal structures. Thermal analysis was done to calculate the weight loss and phase stability at different temperatures. It showed complete crystallization of the yttrium boride around 800^0C. Field emission scanning electron microscopy (FE-SEM) images showed the agglomerated particle morphology. Energy dispersive spectroscopy (EDS) indicated the presence of Y and B elements. Transmission electron microscopy (TEM) images revealed the particle size in the order of 40 nm to 60 nm. Selected area electron diffraction (SAED) pattern were in consensus with XRD results ensuring the formation of nano-sized yttrium boride. The overall results confirmed that yttrium boride can be synthesized by the low-temperature metallothermic reduction process.

***Keywords**: Metallothermic reduction; Yttrium boride; XRD; Microstructure studies; Thermal analysis*

1. Introduction

Yttrium (Y) is one of the important heavy rare earth element and has been widely used in permanent magnetic materials, advanced rare earth alloys, and high-tech materials. Yttrium has a soft, silver-metallic, lustrous, and high crystalline appearance. It is a D-block element with atomic number 39 in the third group. Even though yttrium appears in the transition element series, existence and the chemical properties of the yttrium match with that of lanthanides series and therefore it is considered as a rare earth element [1, 2]. Oxide and boride phases are most common among yttrium and find major industrial applications since both are stable at higher temperatures. Yttria addition in metals improves the mechanical and tribological properties. Also, yttria plays a significant role in oxidation resistance. Rare earth borides are promising refractory with high chemical and thermal stability, low evaporation rate at high temperature, low electronic work function, high and constant electrical conductivity, high transmission stability, high current and voltage capability, and high neutron absorbability [3, 4]. Rare earth borides are utilized as a thermionic emitter to offer higher brightness with lower energy spread and longer service life than tungsten cathodes in electronic devices as well [5, 6]. Yttrium boride is a crystalline material composed of various proportions of yttrium and boron, such as YB_2, YB_4, YB_6, YB_{12}, YB_{25}, YB_{50}, and YB_{66}. They are all grey-colored hard solids having high melting temperatures. The most common form is the yttrium tetraboride (YB_4) and yttrium hexaboride (YB_6). YB_4 has a tetragonal crystal structure, whereas YB_6 has a cubic crystal structure. Yttrium boride exhibits high hardness with high bulk modulus, high melting point, and excellent thermal stability [7]. It has a congruent melting temperature of

*Corresponding author: raman@nitt.edu

https://doi.org/10.2298/JMMB190315048S

2800^0C in YB_4 phase [3], and its oxide form Y_2O_3 has also a high melting point of 2415^0C. Among the various yttrium boride phases, YB_4 gives the best mechanical properties [8, 9]. It can be adopted for high temperature and wear resistance applications. Its high boron content makes it suitable for neutron absorber applications in advanced nuclear reactors as exhibited by other rare earth borides [10, 11].

The properties of many conventional materials change abruptly when formed in the nano range. This is typically because nanoparticles (NPs) have a greater surface area per weight than larger particles which causes them to be more reactive with the other molecules. Ceramic nanoparticles such as silicon carbide, titanium carbide, titanium diboride, and zirconia, dispersed in metal matrix, produce strong lightweight materials with superior mechanical properties [12-14]. Rare earth based nanoparticles find their major applications in biomedical industries [15]. In addition to this, it can be reinforced in metals which find applications in nuclear, thermal, and mechanical engineering. Conventionally, ceramics RE powders and NPs are synthesized by solid-state reduction method, arc melting process, combustion synthesis, sol-gel, and co-precipitation technique. For biological applications, wet chemical methods are usually preferred to yield uniform size distribution of the powders. All these methods have their own advantages and limitations. A brief summary of the various techniques is presented in Table 1.

The addition of borides as dispersoid helps in improving the performance and properties of the materials because of its hard phases with high bulk modulus [26, 27]. There have been some investigations where the effects of rare earth (RE) elements on the solidification, eutectic transformation, and mechanical properties of the steels were investigated [26], and it has been pointed out that the addition of RE contributes to the improvement of the tensile strength and toughness of the light metals and steels [28-30]. Based on the previous exploration, the advantages of the addition of boron and rare earth are worth combining in the preparation of rare earth borides and thereby achieving the strengthening of light metals and steels targeting wear resistance applications. Ceramics of rare earth with higher mechanical properties can be effectively used as a reinforcement phase in lower volume fraction for the fabrication of lightweight metal matrix composites (for example Mg and Al metal matrix composites) [31]. Apart from these applications of high hardness and wear resistance, because of its neutron absorption capability it can be tried in the nuclear application as well. Rare earth based ceramics also find application as thermal barrier coatings (TBCs) in hypersonic vehicles, turbine engines due to its thermal stability and oxidation resistance [32-34]. Yttrium boride nanoparticulate improves corrosion and wear behavior of many commercially available materials such as alloy steels, Co-based alloys, cast white iron, light metals, and zircaloy [35].

As discussed in Table 1, all the conventional techniques adopted have their own limitations. Solid state mixing involves extensive high energy mechanical mixing and a subsequent heat treatment at very high temperature leading to irregular morphologies [16, 17]. Such morphologies, when used as reinforcement phase to metals, will have a significant effect on their mechanical properties [36].

A wet chemical technique such as sol-gel method involves low temperature but the precursors are expensive and also, bulk ceramic fabrication is not possible [16, 17]. Co-precipitation method gives low yield and it involves long holding time [21]. Arc or induction melting process involves very high operating temperature leading to hard particle agglomerates [16]. High temperature and lower yield were major drawbacks that were found from the previous research. Molten salt synthesis is one of the methods which utilizes the eutectic temperature of the salt fluxes and brings down the operating temperature below 1000^0C [24]. This process can be carried out under mild conditions without the need for any special reaction vessels [25]. In this process, the reactants and fluxes are heated in a furnace. Platinum, alumina, or zirconia crucible is usually used in a laboratory experiment [24]. The heating conditions such as temperature and duration are determined by the desired powder characteristics based on the applications. In general, the rate of material transport is increased with an increase in heating temperature. At the same time, the salt evaporation increases as well. The heating duration is determined by the reaction rate, the size and shape of the product particles. Typical temperatures are between 800°C to 1100°C with a duration of 30 to 60 min and even higher duration based on the required salt size and properties [24]. In another method, instead of adding molten salts, pure metal powders, which are reducing in nature, are added along with the reactants in order to reduce the oxide formation. This technique can be adopted for synthesizing boride based ceramic powders. It is known as metallothermic reduction process.

Accordingly, in the present study, nano-yttrium boride particulates in the size range of 40 to 60 nm were synthesized by using metallothermic reduction process using yttria (Y_2O_3) and boron oxide (B_2O_3) as the starting materials, and calcium (Ca) as reductant. Ca is chosen as reductant ahead of magnesium (Mg) since the Ellingham diagram with standard free energy demonstrates that calcium has the best tendency for oxide formation. In fact, it has the lowest

Table 1. *Various synthesis routes*

Method	Process involved	Advantages	Limitations	Reference
Solid State Reaction	High energy mechanical mixing	Well established	Irregular morphologies	[16-18]
	Heating at a very high temperature	Higher productivity	High temperature involved	
Sol-Gel	Precursor suspension	Lower temperature	precursors are expensive	[16, 17, 19]
	Gelation	Uniform particle morphology	Bulk fabrication is not possible	
	Drying and sintering			
Hydrothermal	Reactant mixed with water	Good quality crystals can be grown	Expensive autoclaves	[17, 20]
	Fired at a lower temperature	Crystalline phase can be easily created	Low yield	
	Cooling and washing			
Co-precipitation	Mixture of the ionic solution	High purity and control of the process	Low yield	[16, 21, 22]
	Nucleation and growth	Lower calcination temperature	Long holding time	
	Precipitation, filtration and calcination		Tedious process	
Arc Melting or Induction Melting	Mixing of raw materials	Simple set up	High operating temperature	[16, 23]
	Melting at a higher temperature	Bulk production	Hard particle agglomerates	
Metallothermic Reduction and Molten salt synthesis	Grinding of reactants	Lower temperature	Particle agglomeration	[24, 25]
	Flux/reductant addition	Bulk synthesis is possible		
	Heating at a lower temp.			

free energy among all the reductant metals and hence, it is considered as one of the best deoxidizing agents. The vapor pressure of calcium is adequately high, which permits a successful vapor stage calciothermic reduction of the reactants [37, 38]. The utilization of magnesium is likewise feasible because of its lower oxygen affinity. It is thermodynamically expected that the oxygen concentration under the Mg–MgO equilibrium will be higher than that of Ca–CaO. So, the calciothermic reduction of related oxides will be more favourable than magnesiothermic reduction [38, 39]. The secondary reason for choosing Ca as reductant over Mg is the quantity of the used reductant. In case of Mg, the quantity is always taken 15 to 20 % in excess to the stoichiometric quantity in order to achieve complete reaction. But in case of Ca, due to its low free energy, the reaction is more spontaneous, and the amount of reductant taken is the same amount of the stoichiometry of the reaction [39]. Yttrium boride nanoparticle is not a commercially available one. The synthesis of YB_4 was not explored thoroughly in the past. Few studies have mentioned the synthesis of YB_4 through borothermal reduction method, vacuum thermal reduction method [33], and molten salt synthesis method [40]. In Molten salt route, synthesis of yttrium boride was achieved by using chloride-based reactants along with a boron source [40]. In this present work, a new approach to synthesize YB_4 through the metallothermic reduction process is proposed. This method has not been reported in any of the previous research to the best of our knowledge.

2. Materials and Methods

2.1. Materials

In the present study, the starting materials were the reactant powders and reductant metal. Yttria (Y_2O_3-99.9% Purity) purchased from Indian Rare Earth Ltd and melted boron oxide (B_2O_3-98.4% Purity) supplied by A.B. Enterprises, India, were used as reactant materials. Calcium metal (98% Purity) purchased from Loba Chemie, India, was used as the reductant for this experiment. The results in Figure 1 and Figure 2 illustrate the respective XRD pattern and SEM morphology of the starting reactant materials. X-ray diffraction shows the clear crystalline pattern of Y_2O_3 (JCPDS Ref. 10-4015) and the absence of major B_2O_3

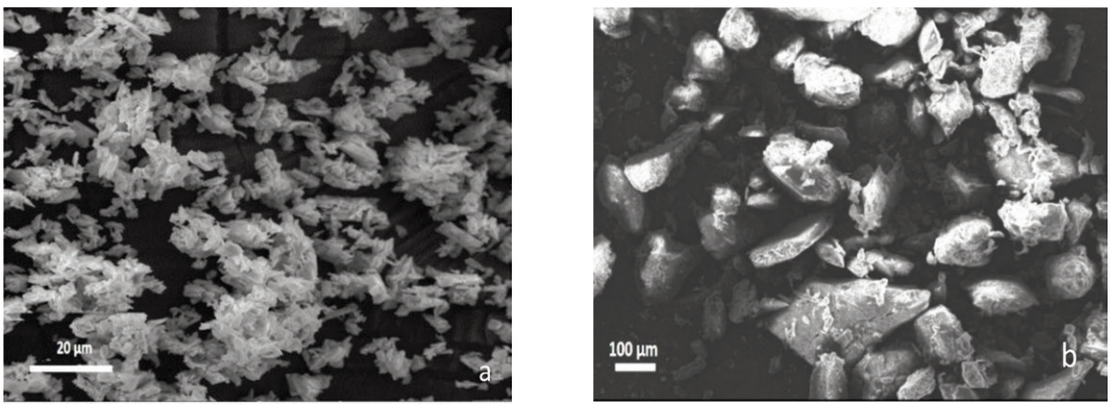

Figure 1. *SEM micrographs of (a) Y_2O_3 (b) B_2O_3*

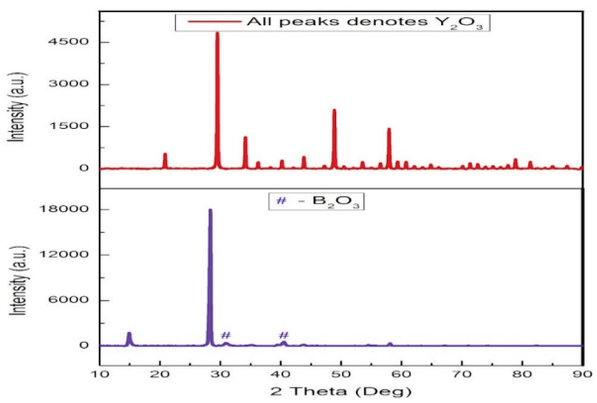

Figure 2. *XRD pattern of Y_2O_3 and B_2O_3*

peak is due to its amorphous nature, (JCPDS Ref. 01-4332). The SEM morphology of yttria shows the particle size in the range of 5 µm and B_2O_3 particles are in the range of 50 µm.

2.2. Synthesis of yttrium boride

The product yttrium boride (YB_4) was obtained from metallothermic reduction route. The steps involving in this synthesis are explained in Figure 3, below. The reactant powders and calcium metal were weighed and taken in the stoichiometric ratio based on the molecular weight from their balanced chemical equations. The chemical equation corresponding to the quantity of powders taken is given below. For 100 g of yttrium boride product, the reactants taken were 85.437 g of Y_2O_3, 105.3606 g of B_2O_3, and 227.457 g of Ca.

$$Y_2O_3 + 4B_2O_3 + 15Ca \rightarrow 2YB_4 + 15CaO \qquad (1)$$

The raw materials were thoroughly grounded in an agate mortar and pestle. Calcium was used as reductant to form calcium oxide by reducing the reactants. The reductant and reactant powders were then loaded into an alumina crucible in an alternative layered manner with Ca reductant at the top and bottom most layer. The crucible with the loaded salts was kept in the muffle furnace and heated at 950^0C for 8 hours under argon atmosphere passed at 150 mL/min. Then the reacted powders were allowed to cool inside the furnace until it attained room temperature. The compound thus obtained was washed with 1M HCl diluted with distilled water followed by warm water washing steps until it got neutral. Once the compound attained neutrality it was filtered using whatman filter paper and dried using a hot plate until the moisture got removed completely. The dried nanopowders were ball milled to remove agglomeration. Ball milling was done in a high energy planetary ball mill (FritschTM Pulverisette 5 Classic Line) with a speed of 250 rpm. The ball-to-powder weight ratio (BPR) was 10:1. The container used was zirconia vial with a capacity of 500 mL and milling media was zirconia balls with a diameter of 10 mm.

2.3. Powder characterization

2.3.1. X-ray studies

X-ray fluorescence (XRF, XGT-5200, Horiba) study was done to ensure the presence of elements along with the composition. X-ray diffraction study

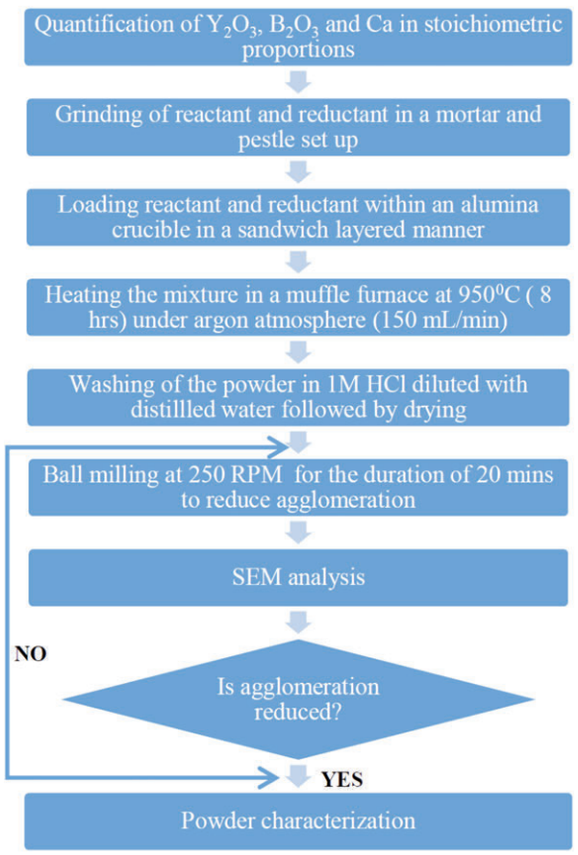

Figure 3. *Process flow chart followed in the synthesis of yttrium boride*

(XRD) was performed using PANalytical XRD (PW3040/60) set up to analyze the formation of yttrium boride phase and to identify the crystal structure. The powder samples were exposed to Cu Kα radiation of wavelength λ=1.54056 Å with a scan rate of 5^0/min. The Bragg angles and the values of the interplanar spacing, d, obtained were subsequently matched with the standard values of YB_4 and YB_6 phases. The average crystallite size (D_{hkl}) of the ceramic powders was determined from the broadening of the diffraction line (2 1 1) of the tetragonal phase using the Scherrer equation. It was determined from the obtained value of full width at the half maximum (FWHM)

$$D_{hkl} = K\lambda/\beta\cos\theta \text{ [41, 42]} \quad (2)$$

D_{hkl} is the crystallite size in the direction perpendicular to the lattice planes, hkl are the Miller indices of the planes being analyzed, K is the Scherrer constant, λ is the wavelength of the X-rays, β is the FWHM of the X-ray diffraction peak in radians, and θ is the Bragg angle. K is taken 0.9 and λ is taken as 0.154056 nm.

2.3.2. Thermal studies

The phase stability and weight loss were analyzed by using thermal analysis test. Thermogravimetry and differential thermal analysis (TG-DTA) was performed in the simultaneous thermal analyzer (STA 8000, Perkin Elmer). The analysis for the compound formation was carried out at a range of 25^{0}C to 1500^{0}C under the nitrogen atmosphere at the rate of 5^{0}C/min with Al_2O_3 as a reference.

2.3.3. Microstructural studies

To ensure the morphology, particle size, microstructure of the obtained yttrium boride compound, field emission scanning electron microscopy (FE-SEM, SUPRA 55VP, Carl Zeiss) was used. Energy dispersive spectroscopy (EDS) to detect the chemical composition in atomic and weight percentages. The crystalline nature, shape, and size of the obtained nano-sized yttrium boride were further confirmed by transmission electron microscopy (TEM) and selected area electron diffraction (SAED, Teenai 20 G2, FEI). SEM samples were prepared by dispersing 0.01 g of powder into 25 mL of ethanol, magnetically stirring for 1 h, ultrasonicating for 10 min, drop coating onto a silicon wafer using a micropipette, dried, and then carbon coating. In the case of TEM studies, the samples were drop coated on a copper grid.

3. Results and Discussions

3.1. X-ray fluorescence study (XRF)

XRF results from Figure 4, demonstrate the presence of peak corresponding to Y and Ca elements. The existence of boron is not revealed because of its low atomic number and its corresponding fluorescent X-rays do not reach the detector of the XRF instrument. Also, the low energy boron peak is difficult to quantify. The chemical composition of yttria and calcium oxide is shown in Table 2. Calcium oxide was detected since Ca was added as the reductant during the synthesis.

Table 2. *As-revealed chemical composition of synthesized powders without Boron*

Chemical	Mass %	Mole %
Y_2O_3	67.807	34.343
CaO	32.193	65.657

Note. Boron is not captured due to its low atomic number

3.2. X-ray diffraction study (XRD)

The XRD results of the typical yttrium boride powders are displayed in Figure 5. The results of XRD confirm the formation of yttrium boride peak YB_4 (JCPDS No.07-0057). Presence of YB_6 is also revealed in XRD pattern (JCPDS No.10-1738). The nanopowder exhibits the cubic structure of YB_6 and tetragonal structure of YB_4 as their respective crystal structure. The formation of narrow peak shows the crystallization of the yttrium boride. The sharp peak indicates a highly crystalline nature of YB_4 and YB_6. The reflections are attributed to YB_4 and YB_6 which are the metal boride phases, along with the traces of unreacted impurities namely yttrium oxide (Y_2O_3) and boron oxide (B_2O_3). The weak diffraction peak ascertains the presence of Y_2O_3 which are noticed between 20^0 and 40^0, and it shows the incomplete dissociation of yttria. The minor amorphous humps between 40^0 and 60^0 indicate the characteristic of B_2O_3 raw material. The incomplete reduction of reactants has been reported in the previous research as well [21]. Generally, at low temperature and short time equivalent to low energy input, yttrium oxide and boron oxide did not get completely dissociated. Efforts to dissolve the oxidized phase, by means of acidic or reductive conditions, were ineffective which was also reported in the previous investigations [21]. Oxide byproducts might be initiated by the unstable yttrium species during the washing process as well. It reacts with water during the washing and results in oxide formation [21]. The formation of YB_6 phase is due to its favored thermodynamics during heat treatment. The enthalpy of fusion and heat capacity values obtained from the previous research database for YB_6 phase (ΔH=10783 cal/g atom, C_p=6.514 cal/g atom) is lower than that of YB_4 phase (ΔH=11236 cal/g atom, C_p=6.879 cal/g atom) at the working temperature of 950^0 C [43]. So the free energy for YB_6 phase formation is lower and making it spontaneous at that temperature.

The average crystalline size obtained from the X-ray line broadening of (2 1 1) plane using Scherrer formulae was 47.15 nm. This size is in agreement with the microstructural images which are discussed below.

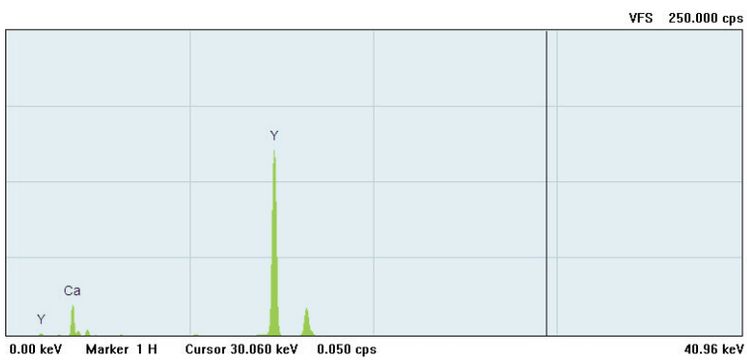

Figure 4. *XRF spectrum of yttrium boride*

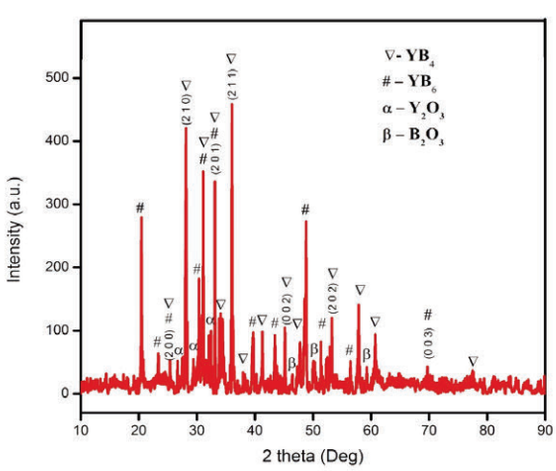

Figure 5. *X-ray diffractogram of yttrium boride*

3.3. Thermogravimetry and differential thermal analysis (TG-DTA)

The thermal behavior of the formation of nano-sized yttrium boride was investigated by TG-DTA. In Figure 6, there is a consistent weight loss of about 7.58% from room temperature to 450^{0}C which attributes to volatilization of moisture that was present in the reactants. It is confirmed by the strong endothermic peak at 131^{0}C. Once the volatilization of water content happens, the beginning of decomposition of oxides takes place which is accompanied by weight loss. At the temperature of 633^{0}C and 704^{0}C, two endothermic patterns are observed because of the decomposition of the reactant oxides. A gradual weight loss can be observed while decomposition of oxides took place. About 13.6% of weight loss occurred after the reactants get dissociated. Weight loss is hardly observed above 800^{0}C, after the decomposition of reactants, which shows the crystallization of the yttrium boride. Also, there is no peak in the DTA curve which is in agreement with the crystallization of yttrium boride. Around 1,228^{0}C a sharp exothermic peak can be witnessed along with a drastic weight loss. It confirms the oxidation of nano-sized yttrium boride at a higher temperature as confirmed in the previous researches [3, 44]. A sudden weight loss of 24% is observed once the compound undergoes oxidation.

3.4. Field emission scanning electron microscopy (FE-SEM) & energy dispersive spectroscopy (EDS)

The SEM image in Figure 7 demonstrates the morphology of yttrium boride. The formation of irregular polyhedral morphology shown in Figure 7 (a) and Figure 7 (b) revealed the existence of nano-sized yttrium boride (YB_4) along with the existence of YB_6 phases. The image also indicated the average size of the particle in the nano range of 40 nm to 60 nm with little agglomerations. The formation of YB_4 phase crystallized first during reduction followed by YB_6 phase which formed because of its favored growth kinetics during the firing process [9]. The crystalline shapes detected are irregular. Different shapes could be attributed to different particle growth mechanism during the reduction process. From the SEM image, the sample prepared at 950^{0}C with Ca metal exhibited irregular shapes and the average size of the particle can be observed in the nano range of 40 nm to 60 nm. The EDS pattern presented in Figure 7 (d) shows the presence of yttrium, boron, and oxygen concentration in their respective weight and atomic percentage. The presence of boron in the final compound indicates the formation of nano-sized yttrium boride. The presence of O shows the availability of few un-dissociated reactants which are yttria and boron oxide. The presence of oxygen might also occur due to the surface oxidation of the powder [45].

3.5. Transmission electron microscopy (TEM)

The TEM image displayed in Figure 8 (a) and Figure 8 (b) further confirms the polyhedral morphology of yttrium boride. It also ascertains the average particle size in the range of 40-60 nm. The bright spots in the selected area electron diffraction (SAED) pattern confirms the crystallization of the nano-sized yttrium boride. The presence of a diffraction spot shows the single crystalline nature of the final compound. The elongation of the bright spot indicates that the powder compound has undergone mechanical working or the deformation in the form of ball milling. The SAED pattern in Figure 8 (c) illustrates Bragg spot at the planes corresponding (2 1 0), (2 1 1), (0 0 2), and (0 0 3) coincides with the d-spacing of the XRD results. The first ring, second ring, and the third ring with the equivalent d-spacing of ~3.200 Å, ~2.40 Å and ~0.190

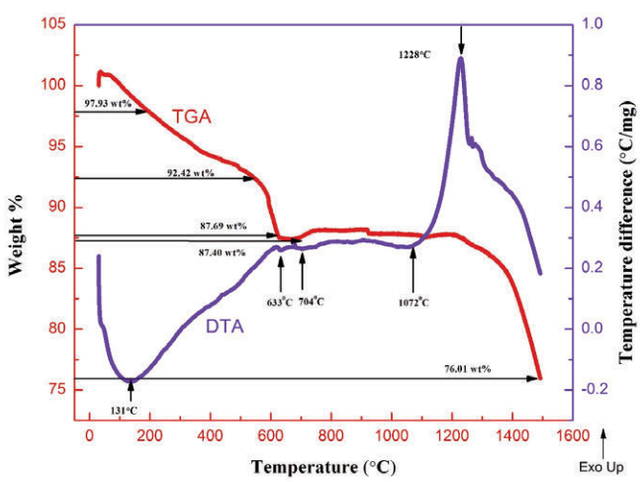

Figure 6. *TG and DTA for yttrium boride formation*

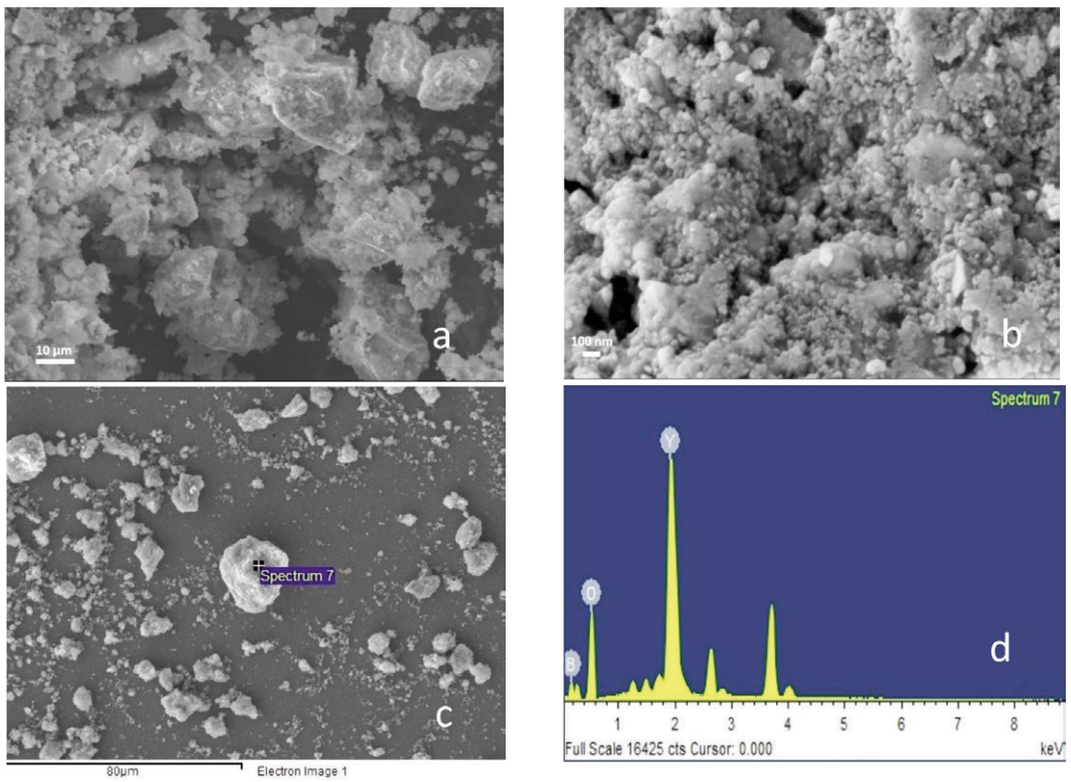

Figure 7. *FE-SEM micrographs of yttrium boride (a) at 20 K X magnification (b) at 300 K X magnification (c) Image of the EDS spectrum spot-7 (d) EDS spectrum*

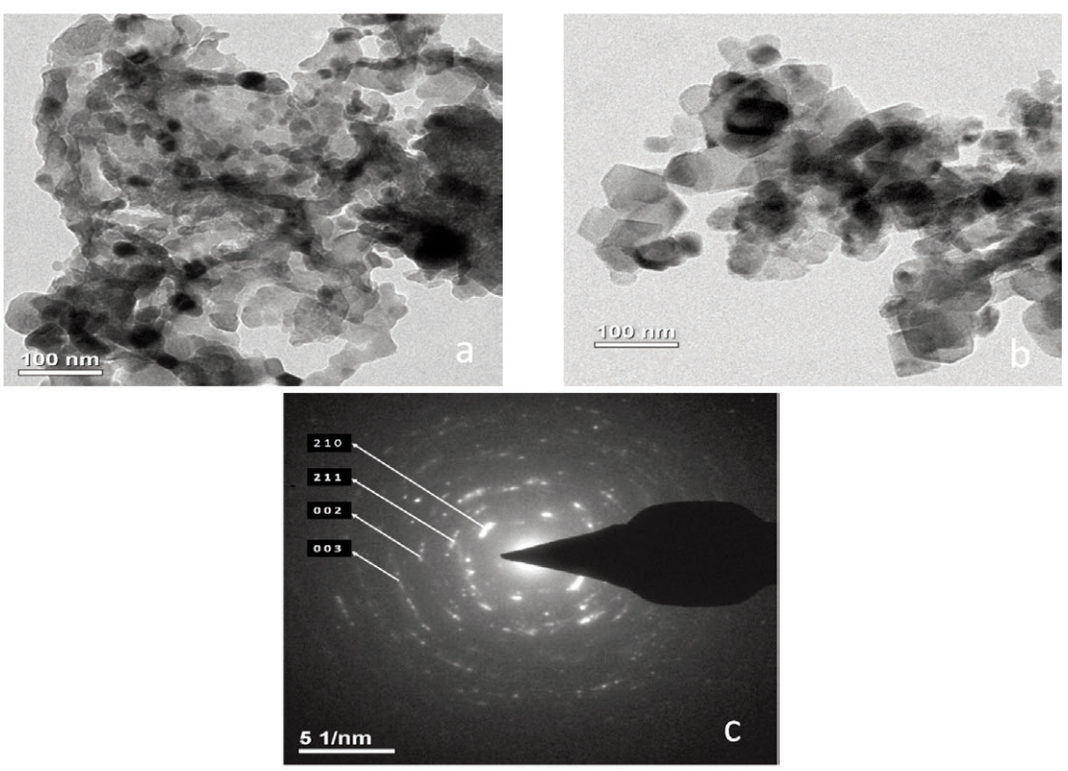

Figure 8. *(a) & (b) TEM images of yttrium boride (c) Diffraction pattern*

Å respectively correspond to (2 1 0), (2 1 1), and (0 0 2) reflection planes. These (h k l) values match with XRD results for YB_4 phase. The fourth ring with equivalent d-spacing of ~1.38 Å corresponds to (0 0 3) reflection plane. It matches with XRD results for YB_6 phase.

3.6. Byproducts and its influence on the final chemical composition of powders

Byproducts are usually formed due to the addition of fluxes or reductant during the process and also because of the high processing temperature. Ineffective and insufficient acid washing is the reason for the residual of reductant oxides [5]. Due to the formation of oxide-based byproducts the desired properties such as mechanical, thermal resistance property, neutron absorbing capacity are not achieved. These reactant/reductant oxides need to be reduced in the final composition in order to achieve effective synthesis and higher yield of rare earth boride. From the literature search, the synthesis of other rare earth boride powders was found to produce several byproducts with oxygen contents in higher concentration. Previously, higher oxygen content was found during the synthesis of GdB_4 by B_4C reduction method [34]. Also, synthesis of LaB_6 using B_4C reduction method reported reactant oxide phase in the EDS result [11]. Higher oxygen has been found during the synthesis of nickel boride and yttrium boride prepared by molten salt synthesis route [40]. CeB_6 prepared by high-temperature self-propagating synthesis method also indicated the reductant oxide phase in the EDS. In this work, considerable amount of reductant was used (higher than the calculated stoichiometric amount) to increase the yield of CeB_6 [46].

4. Conclusions

In the present study, nano-sized yttrium boride powders were successfully synthesized through the metallothermic reduction route using yttria and boron oxide as reactant materials and calcium as a reductant. The synthesis temperature (950^0C) was much lower than the conventional solid-state mixing and arc or induction melting process. Also, the bulk fabrication of the product was achieved in this study. The primary conclusions of the present experimental findings are as follows:

Presence of elemental constituents was noticed in the synthesized nano-yttrium boride compound by XRF analysis.

Through XRD studies, the formation of YB_4 and YB_6 phases was confirmed. It also indicated the tetragonal crystal structure for YB_4 phase and cubic structure for YB_6 phase. Moderate amounts of raw materials remained undissociated in the final compound which was also reflected in the XRD peaks. The average crystalline size measured using the FWHM value through Scherrer formulae for diffraction line (2 1 1) was 47.15 nm.

TGA-DTA results indicated the crystallization of nano-yttrium boride was attained above 800^0C with the absence of DTA peak and no considerable weight loss in TGA pattern. This result also revealed that the yttrium boride underwent oxidation above $1,228^0$C.

SEM images showed the irregular polyhedral morphology of YB_4 and YB_6 phase. The image also indicated the average size of the particle in the nano range of 40 nm to 60 nm (with agglomeration). The formation of YB_6 phase was due to its favored thermodynamics and growth kinetics during the heat treatment process. EDS pattern exposed the presence of yttrium, boron, and oxygen concentration.

TEM images showed the morphology of the nano-sized yttrium boride and the particle size was in the range of 40 nm to 60 nm. SAED pattern matched with d-spacing values of the XRD results to reassure the formation of yttrium boride. Presence of bright spot indicated the crystalline nature of the product.

In the present study, even though byproducts with oxygen content were found to be present, it is possible to reduce their concentration, if a design of experiment approach is chosen to find the effect of processing temperature and quantity of reductant on the final yield and purity of powders, and the study is on-going. Further, the synthesized powders can be used as a reinforcement phase to fabricate lightweight metal matrix composites and the study is ongoing.

Acknowledgment

The authors sincerely thank all the project staff in the ElectroPyro Metallurgy Division at CSIR-Central Electro Chemical Research Institute, Karaikudi for the experimental facilities extended during this research work. Also, the authors would like to thank researcher Mr. S.A.Srinivasan for his help during this work.

References

[1] T. Damhus, R.M. Hartshorn, A.T. Hutton, Nomenclature of Inorganic Chemistry: IUPAC Recommendations 2005. Cambridge: Royal Society of Chemistry, 2005, p. 51.

[2] W. Yang, W. Yingjun, D. Jinge, W. Zhanghong, W. Qinglian, J. Rare Earth 34 (7) (2016) 747-756.

[3] J.A. Zaykoski, M.M. Opeka, L.H. Smith, I.G. Talmy, J. Am. Ceram. Soc. 94 (11) (2011) 4059-4065.

[4] H. Kotan, Mat. Sci. Eng. A, 647 (2015) 136-143.

[5] D. Ağaoğullari, Ö. Balci, İ. Duman, M. Lütfi Öveçoğlu, 22nd International Conference on Metallurgy and

Materials 17. 5. 2013, Brno, Czech Republic, 2013.

[6] R.K. Selvan, I. Genish, I. Perelshtein, J.M. Moreno, J. Gedanken, Phys. Chem. C, 112 (2008) 1795-1802.

[7] A. Waskowska, L. Gerward, J. Staun Olsen, K. Ramesh Babu, G. Vaitheeswaran, V. Kanchana, A. Svane, V.B. Filipov, G. Levchenko, A. Lyaschenko, Acta Mater., 59 (2011) 4886-4894.

[8] S. Otani, M.M. Korsukova, T. Mitsuhashi, N. Kieda, J. Cryst. Growth, 217 (2000) 378-382.

[9] N. Sekido, T. Ohmurab, J.H. Perepezkoc, Intermetallics, 89 (2017) 86-91.

[10] R. Kanakala, G. Rojas-George, O.A. Graeve, J. Am. Ceram. Soc., 93(10) (2010) 3136-3141.

[11] J.K. Sonber, K. Sairam, T.S.R.Ch. Murthy, A. Nagaraj, C. Subramanian, R.C. Hubli. J. Eur. Ceram. Soc., 34 (2014) 1155-1160.

[12] S. Das, M. Chandrasekaran, S. Samanta, Mater. Today Proc., 5(9) (2018) 18110-18119.

[13] M. Sheikhzadeh, S. Sanjabi, Mater. Design, 39 (2012) 366.

[14] M. Darabara, G. D. Papadimitriou, L. Bourithis, Mater. Sci. Tech-Lond., 23(7) (2007) 839-846.

[15] A. Escudero, A.I. Becerro, C. Carrillo-Carrion, Nuria O. Nunez, Mikhail V. Zyuzin, M.. Laguna, D. Gonzalez-Mancebo, M. Ocana, W.J. Parak, Nanophotonics, 6(5) (2017) 881-921.

[16] Z. Cai, X. Xing, L.Li, Y. Xu, J. Alloy. Compd., 454 (2008) 466-470.

[17] J.-S. Lee, Mater. Sci-Poland, 31(2) (2013) 240-245.

[18] G. Blasse, L.H. Brixner, Chem. Phys. Lett., 173 (1990) 409-411.

[19] M. Baran, Ya. Zhydachevskii, A. Suchocki, A. Reszka, S. Warchol, R. Diduszko, A. Pajaczkowska, Opt. Mater.,34 (2012) 604-608.

[20] B. Basavalingu, H.N. Girish, K. Byrappa, Kohei Soga, Mater. Chem. Phys., 112 (2008) 723-725.

[21] Y. Wang, J. Ma, J. Tao, X. Zhu, J. Zhou, Z. Zhao, L. Xie, H. Tian, Mater. Lett., 60 (2006) 291-293.

[22] M. Dambekalne, M. Antonova, M. Livinsh, B. Garbarz-Glos, W. Smiga, A. Sternberg, J. Eur. Ceram. Soc., 26 (2006) 2963-2966.

[23] M. Johari Abu, J. Juliewatty Mohamed, Z. Arifin Ahmad, Int. J. Refract. Met. H,47 (2014) 86-92.

[24] T. Kimura, Advances in ceramics - synthesis and characterization, processing and specific applications, INTECH Open Access Publisher (2011) p. 75.

[25] Z. Huang, F. Li, C. Jiao, J. Liu, J. Huang, L. Lu, H. Zhang, S. Zhang, Ceram. Int., 42 (2016) 6221-6227.

[26] W. Shen, B. Nan, W. Wang, L. Yu, Q. Zhang, Y. He, X. Huang, G. Yuan, J. Alloy. Compd., 738 (2018) 363-371.

[27] H.B. Michael Rajan, S. Ramabalan, I. Dinaharan, S.J. Vijay, Mater. Design, 44 (2013) 438-445.

[28] A.P. Gulyayev, Ya. A. Ul'yanin, Met. Sci. Heat Treat., 3 (9-10) (1961) 460-464.

[29] R. Tuttle, Int. J. Metalcast., 6(2) (2012) 51-65.

[30] S.A. Bagaber, T. Abdullahi, Z. Harun, N. Daib, M. Hafiz D. Othman, Arab. J. Sci. Eng., 42 (2017) 4559-4564.

[31] Meenashisundaram G.K, Gupta M, JOM The J. of the Min. Met. and Mater. Soc., 68 (7) (2016) 1890-1901.

[32] G. Di Girolamo, F. Marra, M. Schioppa, C. Blasi, G. Pulci, T. Valente, Surf. Coat. Tech., 268 (2015) 298-302.

[33] G. A. Meerson, N.N. Zhyravlev, R. M. Manelis, A. D. Runov, A. A. Stepanova, L. P. Grishina, and N. V. Gramm, News Acad. Sci. USSR Inorg. Mater. (Izvestiya Akademii Nauk SSSR: Neorganicheskiye Materialy), 2(4) (1966) 608.

[34] J. Kumar Sonber, T. Shri Ram Chandra Murthy, K. Sairam, V. Kain, J. Korean Ceram. Soc., 54(2) (2017) 121-127.

[35] H. Ahmadiand, M. Nouri, J. Mater. Sci. Technol, 27 (9) (2011) 851-855.

[36] G. Kumar Meenashisundaram, M. Hoon Nai, A. Almajid, K. Abdelrazek Khalil, H.S. Abdo, M. Gupta, J. Alloy. Compd., 664 (2016) 45-58.

[37] B. Bertheville, J.E. Bidaux, J. Alloy. Compd., 387 (2005) 211-216.

[38] Z. Xing, J. Lu, X. Ji, Small methods, 2 (2018) (1800062) 1-13.

[39] D. Ağaoğulları, Ö. Balcı, M. Lütfi Öveçoğlu, İ.Duman, Kona Powder Part. J., 33 (2016) 203-219.

[40] G. Gouget, P. Beaunier, D. Portehault, C. Sanchez, Faraday Discuss., RSC, 191 (2016) 511-525.

[41] M. Bellardita, A. Di Paola, B. Megna, L. Palmisano, J. Photoch. Photobio. A, 367 (2018) 312-320.

[42] R. Mahendran, S. P. Kumaresh Babu, S. Natarajan, A. Vallimanalan, S. Manivannan. Ceram. Int., 43(11) (2017) 8051-8056.

[43] O.H. Krikorian, Estimation of heat capacities and other thermodynamic properties of refractory borides, Lawrence Radiation Laboratory, California, USA, 1971, p. 27.

[44] E. M. Levin and H. F. McMurdie, Phase diagrams for ceramists, 1975 supplement, The Am. Cera. Soc., Columbus, OH, USA, 1975, p. 48.

[45] R. Kalai Selvan, I. Genish, I. Perelshtein, J.M. Calderon Moreno, A. Gedanken, J. Phys. Chem. C, 112 (2008) 1795-1802.

[46] D. Zhihe, Z. Tingan, G. Yongnan, H. Jicheng, J. Rare Earth, 30 (11) (2012) 1129-1133.

NOVI POSTUPAK ZA DOBIJANJE NANOČESTICE ITRIJUM BORIDA PUTEM MATALOTERMIČKOG REDUKCIONOG PROCESA

M. Sadhasivam [a], L. J. Berchmans [b], G. K. Meenashisundaram [c], U. Mehana Usmaniya [b], S. R. Sankaranarayanan [a,*], S.P. Kumaresh Babu [a]

[a] Nacionalni tehnološki institut, Katedra za metalurško i inženjerstvo materijala, Tiručirapali, Tamil Nadu, Indija

[b] Savet za naučno i industrijsko istraživanje – Centralni institut za elektrojemiska istraživanja, Odeljenje za piro-elektro metalurgiju, Karaikudi, Tamil Nadu, Indija

[c] Institut za proizvodnju i tehnologiju u Singapuru, Grupa za razvoj tehnologije, Singapur

Apstrakt

U ovom radu je prikazan novi način za dobijanje nanopraha itrijum borida (YB_4) metodom metalotermičke redukcije. Polazni materijali su bili itrijum oksid (Y_2O_3) i boron oksid (B_2O_3) koji su korišćeni kao reaktanti, i kalcijum (Ca) koji je korišćen kao reducent. Reakcija je izvedena na 950°C u prisustvu argona, a nakon toga je usledilo ispiranje kiselinom. Dobijeni proizvod je podvrgnut analizi rentgenske fluorescencije (XRF) koja je pokazala njegove elementarne konstituente, kao i čistoću dobijenih nanoprahova. Rentgenska difrakcija (XRD) je pokazala formiranje YB_4 i YB_6 faza, kao i njihovu kristalnu strukturu. Termalna analiza je izvedena da bi se izračunao gubitak mase, kao i stabilnost faza na različitim temperaturama. Ova analiza je pokazala da je došlo do potpune kristalizacije itrijum borida na 800°C. Skenirajuća elektronska mikroskopija za emitovanje polja (FE-SEM) je pokazala da je morfologija čestica grozdastog oblika. Energijsko disperzivna spektroskopija (EDS) je naznačila prisustvo Y i B elemenata. Transmisionim elektronskim mikroskopom (TEM) je ustanovljeno da je veličina čestica između 40 i 60 nm. Elektronske difrakcije sa odabrane površine (SAED) su se poklopile sa rezultatima rengenske difrakcije i potvrdile formiranje nanočestica itrijum borida. Ukupni rezultati su potvrdili da itrijum borid može da se sintetiše prilikom postupka metalotermičke redukcije na niskim temperaturama.

***Ključne reči**: Metalotermička redukcija; Itrijum borid; XRD; Ispitivanje mikrostrukture; Termalna analiza*